E1-2008-54

S. R. Hashemi-Nezhad[1], I. V. Zhuk[2], M. Kievets[2],
M. I. Krivopustov[3], A. N. Sosnin[3], W. Westmeier[4], R. Brandt[4]
(On behalf of «Energy plus Transmutation» Collaboration)

INVESTIGATION OF SPATIAL DISTRIBUTION OF FISSION-RATE OF NATURAL URANIUM NUCLEI IN THE BLANKET OF ELECTRONUCLEAR SETUP «ENERGY PLUS TRANSMUTATION» AT DUBNA NUCLOTRON PROTON BEAM AT ENERGY 1.5 GeV

Submitted to «Nuclear Instruments and Methods»

[1]School of Physics, A28, University of Sydney, NSW 2006, Australia
[2]Joint Institute of Power and Nuclear Research-Sosny NASB, Minsk, Belarus
[3]Joint Institute for Nuclear Research, Dubna
[4]Fachbereich Chemie, Philipps University, Marburg, Germany

Хашеми-Нежад С. Р. и др.
(от коллаборации «Энергия плюс трансмутация»)
E1-2008-54

Исследование пространственного распределения скоростей деления ядер естественного урана в составе бланкета электроядерной установки «Энергия плюс трансмутация» на протонном пучке нуклотрона ОИЯИ при энергии 1,5 ГэВ

Эксперимент выполнен на установке «Энергия плюс трансмутация» (Лаборатория физики высоких энергий им. В. И. Векслера и А. М. Балдина ОИЯИ, Дубна), которая представляет собой свинцовую мишень (диаметр 8,4 см, длина 45,6 см), окруженную урановым бланкетом (206,4 кг естественного урана). Полиэтиленовая защита со слоем кадмия окружает сборку «мишень плюс бланкет» и изменяет спектры нейтронов расщепления (spallation) и деления. Установка облучалась на протонном пучке ускорителя нуклотрон с энергией 1,5 ГэВ. В работе представлено сравнение пространственных распределений скоростей деления ядер естественного урана в установке и бланкете, полученных экспериментально и рассчитанных методом Монте-Карло с использованием программы MCNPX 2.6C. Кроме делений, индуцированных нейтронами, расчет включал также следующие реакции: $^{\mathrm{Nat}}\mathrm{U}(p,f)$, $^{\mathrm{Nat}}\mathrm{U}(\pi,f)$ и $^{\mathrm{Nat}}\mathrm{U}(\gamma,f)$. Между экспериментальными и расчетными значениями наблюдается хорошее согласие. Подробно обсуждаются возможные источники погрешностей результатов эксперимента и расчета.

Работа выполнена в Лаборатории физики высоких энергий им. В. И. Векслера и А. М. Балдина ОИЯИ.

Препринт Объединенного института ядерных исследований. Дубна, 2008

Hashemi-Nezhad S. R. et al.
(On behalf of «Energy plus Transmutation» Collaboration)
E1-2008-54

Investigation of Spatial Distribution of Fission-Rate of Natural Uranium Nuclei in the Blanket of Electronuclear Setup «Energy plus Transmutation» at Dubna Nuclotron Proton Beam at Energy 1.5 GeV

The «Energy plus Transmutation» experimental setup of the Veksler and Baldin Laboratory of High Energy Physics within the Joint Institute for Nuclear Research (JINR) in Dubna, Russia, is a lead target (with a diameter of 8.4 cm and length of 45.6 cm) surrounded by a uranium blanket (weight 206.4 kg of natural uranium). A polyethylene plus cadmium shield is placed around the target-blanket assembly to modify the spallation and fission neutron spectra in the system. The setup was irradiated by a proton beam of energy 1.5 GeV using the Nuclotron accelerator. In this work the spatial distribution of natural uranium fission-rate in the assembly and fission-rate in the blanket was determined experimentally and compared with Monte-Carlo predictions using the MCNPX 2.6C code. Besides neutron-induced fission the calculations include the $^{\mathrm{Nat}}\mathrm{U}(p,f)$, $^{\mathrm{Nat}}\mathrm{U}(\pi,f)$ as well as $^{\mathrm{Nat}}\mathrm{U}(\gamma,f)$ reactions. Good agreement between the experimental and calculation results was obtained. The possible sources of errors in the experiment and calculations are discussed in detail.

The investigation has been performed at the Veksler and Baldin Laboratory of High Energy Physics, JINR.

Preprint of the Joint Institute for Nuclear Research. Dubna, 2008

INTRODUCTION

Accelerator driven systems (ADS) are considered to be one of the best options for cleaner, safer and economically viable methods for future nuclear energy production and nuclear waste incineration [1–3]. In these systems the spallation neutrons sustain the fission chain reaction under subcritical conditions. These spallation neutrons have an energy spectrum covering a very wide energy range of keV to GeV and are produced via interactions of high energy ions (such as protons) with extended heavy nuclide targets (such as lead, see, e.g., [4]).

The currently available data tables on the reaction cross section for neutrons with energy above 20 MeV are not complete for all elements and isotopes that can be present within an ADS [5]. Therefore, understanding the behavior of spallation neutrons and their interaction with the nuclei present in the system has prime importance. One of the major requirements in the design of an ADS is the ability to simulate the interactions of neutrons and other secondary particles with the nuclei present in the ADS environment and to make appropriate calculations and predictions. In this work the MCNPX 2.6C code (beta version) [6] was used to simulate the interaction of the proton with target material and behavior of the spallation neutrons and other secondary particles in the system.

Determination of fission-rate in an ADS is essential for output power and effective neutron multiplication calculations. The latter is one of the most important parameters of the ADS which is aimed to operate under subcritical conditions.

The experiments reported in this paper were carried out at the Veksler and Baldin Laboratory of High Energy Physics (VBLHEP), Joint Institute for Nuclear Research (JINR), Dubna, Russia, using the Nuclotron accelerator of this institute.

1. EXPERIMENTAL

1.1. Experimental Setup.

1.1.1. Energy plus Transmutation Setup. The experiments were carried out using an experimental assembly in JINR known as «Energy plus Transmutation» setup. Figure 1, *a, b* illustrates the schematic drawings of the «Energy plus Transmutation» installation.

Detailed description of this setup is given elsewhere [7] and in the present paper only a brief explanation of its components and their arrangements is given:

1. The system contains four cylindrical lead targets each with diameter 8.4 cm and length 11.4 cm.

2. A natural uranium blanket surrounds each of the four target sections. Each uranium blanket is composed of 30 uranium rods of diameter 3.6 cm (including the Al-cladding) and length 10.4 cm hermetically sealed in aluminum cladding. The uranium rods are arranged in the form of hexagonal (triangular) lattice with

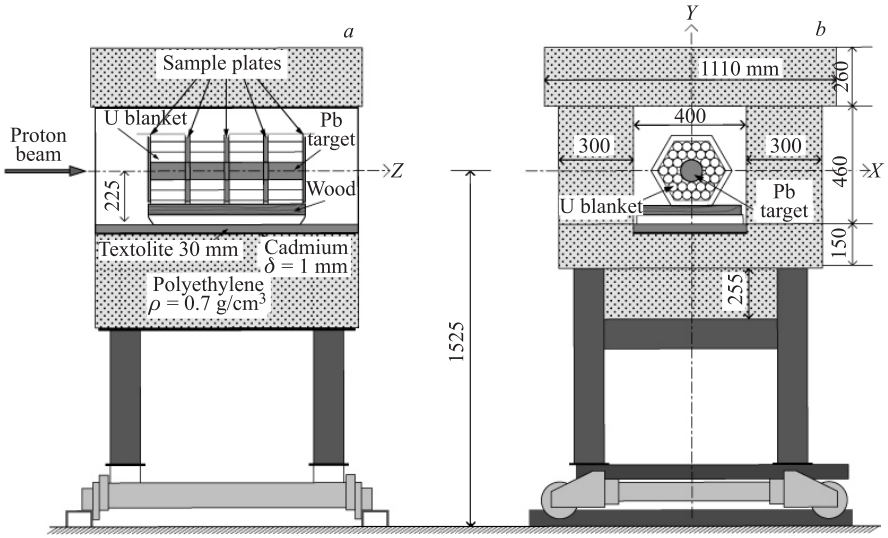

Fig. 1. Schematic drawings of the «Energy plus Transmutation» experimental setup: *a*) *YZ* cross section; *b*) *XY* cross section [7]

pitch size of 3.6 cm. The weight of natural uranium in each blanket section is 51.6 kg and the whole setup contains total of 206.4 kg of natural uranium. Each section of target-blanket is safely fixed within a steel right angle hexagonal prism container. The four target-blanket sections are aligned along the Z-axis (the target axis) with 0.8 cm gap between the sections. These gaps are used to place activation foils, track detectors and other sensors used in the study of the neutron field within the system.

3. The whole target-blanket system was placed within a wooden container filled with granulated polyethylene of average density 0.7 $\mathrm{g \cdot cm^{-3}}$ with dimensions and the arrangements as shown in Fig. 1.

4. The inner walls of the container were covered with a Cd foil of thickness 1 mm.

5. The whole setup is mounted on a platform that can be moved on a rail and its position on the platform can be adjusted with the help of appropriate screw devices.

1.1.2. Fission Sensor Sample. In order to study and determine the fission-rate in the «Energy plus Transmutation» setup, metallic foils of natural uranium (fission-foils) were used as fissionable material (the same material as the blanket). These foils (diameter of 7 mm and thickness of ~ 0.1 mm) were manufactured by cold rolling and vacuum annealing of the material. As the thickness of these foils

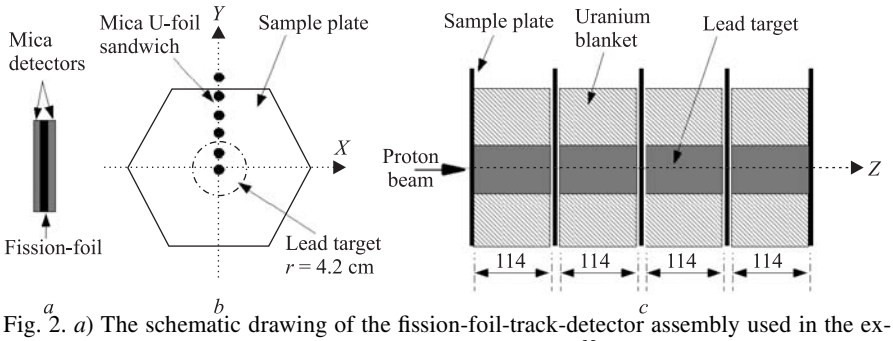

Fig. 2. *a*) The schematic drawing of the fission-foil-track-detector assembly used in the experiments; *b*) schematic drawing of the sample plates and $^{\mathrm{Nat}}$U-mica detector sandwiches used in the experiment; *c*) placement of the sample plate within «Energy plus Transmutation» assembly. Each target section is 114 mm long and there is a gap of 8 mm between each pair of target-blanket sections

was greater than the mean range of the fission fragments in uranium (5.41 μm), the fission-foils are considered to be «thick foils». The fission-foils were placed in close contact between two Fluorophlogopite (artificial mica) track detector sheets as shown in Fig. 2, *a*.

The fission-foil mica sandwiches were mounted on plastic sheets (sample plates) of thickness ~ 0.2 mm, along the $+Y$-axis at different radial distances R (0, 3, 6, 8.5, 11 and 13.5 cm), as shown in Fig. 2, *b*. Five plates each containing six samples were placed in front, back and in the three gaps between the target-blanket sections (Fig. 2, *c*).

1.2. Proton Irradiation. The setup was irradiated by a proton beam of energy 1.5 GeV in direction parallel to the target axis (shown in Fig. 1, *a* and Fig. 2, *c*). The alignment of the beam centre with the centre of the lead target was achieved by examining Polaroid films placed in front of the target and exposed to a couple proton pulses. This type of beam alignment can have an error of a few mm in X- and Y-directions.

Total fluence of the protons striking the target during the main irradiation was determined by activation of an Al-foil via the $^{27}\mathrm{Al}(p,3pn)^{24}\mathrm{Na}$ reaction [8, 9]. The number of the $^{27}\mathrm{Al}(p,3pn)^{24}\mathrm{Na}$ reactions was determined by gamma-ray spectrum analysis of ^{24}Na decay using the properly calibrated HPGe detector. The total number of protons on the system was $(1.17 \pm 0.06) \cdot 10^{13}$ of which $(1.12 \pm 0.05) \cdot 10^{13}$, i.e., 95.8% was on the target [10].

The proton beam intensity distribution along the X- and Y-axes was determined using the reaction $^{\mathrm{Nat}}\mathrm{Pb}(p,f)$ in conjunction with mica track detectors. Sandwiches of natural lead ($^{\mathrm{Nat}}$Pb) foils of dimensions $0.7 \times 0.7 \times 0.03$ cm, in contact with mica detectors (similar to the $^{\mathrm{Nat}}$U-mica sandwiches, Fig. 2, *a*) were

placed on plate 1 in front of the lead–uranium blanket setup in contact with the target (Fig. 2, *c*) along the X- and Y-axes, extending from -13.5 to 13.5 cm in both directions. Total number of these samples was 37. The incident protons ($E_p = 1.5$ GeV) induce fission in $^{\mathrm{Nat}}$Pb and their tracks register in the mica detectors. After exposure the track detectors were etched and track density in each sample was determined (details of the etching and counting procedures will be given in this section). The variations of the track density with distance along the X- and Y-axes were used to obtain the beam intensity distribution.

Figure 3 illustrates the observed beam intensity distributions along the X- and Y-directions. In each of the X- and Y-directions the data were fitted with a Gaussian function and the coordinates of the beam centre (X_c and Y_c) on the target and full width at half maximum (FWHM) of the distributions were obtained from the Gaussian fits as $X_c = (-0.32 \pm 0.03)$ cm, $(\mathrm{FWHM})_X = (2.01 \pm 0.06)$ cm and $Y_c = (-0.14 \pm 0.08)$ cm, $(\mathrm{FWHM})_Y = (3.10 \pm 0.19)$ cm for the X- and Y-axes, respectively.

The secondary neutrons produced in the system can also induce fission in the lead-foils. Contribution of the secondary neutron-induced fission, $^{\mathrm{Nat}}\mathrm{Pb}(n, f)$, to the observed fission events in the mica detectors was negligible compared to that of the $^{\mathrm{Nat}}\mathrm{Pb}(p, f)$ events produced by the primary protons. Examination of the neutron energy distribution at the centre of the plate ($X = 0$, $Y = 0$) and at position of the last lead-mica sample along the $+Y$-direction ($X = 0$ cm, $Y = 13.5$ cm) showed that the contribution of the secondary neutrons with energy greater than 30 MeV (energy range at which $^{\mathrm{Nat}}\mathrm{Pb}(n, f)$ cross section becomes significant [11]) to these spectra is 8.8% and 2.1% at $Y = 0$ cm and $Y = 13.5$ cm, respectively.

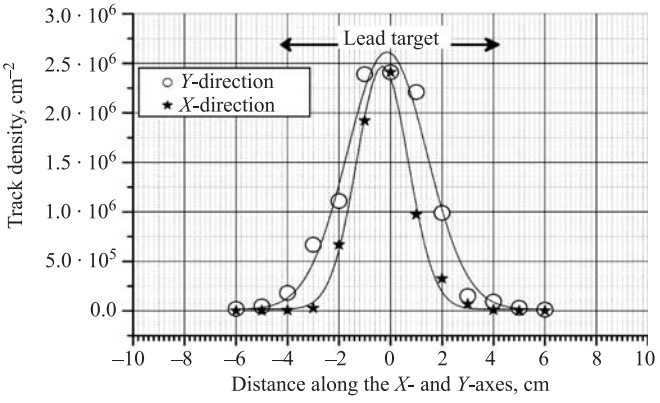

Fig. 3. The beam profile obtained using $^{\mathrm{Nat}}\mathrm{Pb}(p, f)$ reaction and mica track detector (see the text for details)

1.3. Processing of the Mica Detectors. After exposure the mica detectors were etched in 7% HF at 60 °C. The duration of the etching time was decided on the basis of the track population in a given sample. Shorter etching times were used for samples with higher track densities, to minimize the overlapping of the track openings. To obtain an accurate measure of the track densities the tedious method of manual track counting was chosen. We counted tracks in many photomicrographs produced for each mica detector using an optical microscope. Again the overall magnification of the images was decided on the basis of the track population in a given sample. For each foil, the mean of track density (track/cm^2) in two mica detectors on its each side was determined. The accuracy of the track counting was dependent on the track population in a given mica detector.

2. MONTE-CARLO CALCULATIONS

2.1. Calculation Procedure. We used the MCNPX 2.6C (beta version) Monte-Carlo (MC) code [6] to simulate the behavior of protons, neutrons and other secondary particles in our experimental setup. The experimental setup was built into the code with the characteristics given in Fig. 1 and included the natural uranium fission-foils as shown in Fig. 2.

The setup was «irradiated» with a proton beam of energy 1.5 GeV parallel to the target axis and with the beam profile and beam centre coordinates as described in Subsec. 1.2. It was assumed that the projected beam profile on X- and Y-axes is the same as that shown in Fig. 3. The beam acceptance radius (a cylindrical tube in which the proton beam was enclosed) was set to 6 cm to include all protons including those that may hit the system beyond the target. In this case some of the protons (for probabilities, see Fig. 3) may hit the uranium blanket (and thus result in higher neutron multiplicity than in the lead) and some protons may strike the voids between the uranium rods and target (and result in no secondary particle production).

In the simulations each sample plate contained 23 or 31 fission-foils along the Y-axis from $Y = -13.5$ cm to $Y = 13.5$ cm. In order to avoid confusion the fission-foils used in the MC calculations will be referred to as MC-fission-foils and will be abbreviated to MC-FF. Figure 4 shows the experimental setup and sample plates as *seen* by the MC-code.

The following MCNPX options were used in the calculations:

1. Neutrons, protons, pions and photons were transported together with other particles allowed by the code and which could be produced by the incident protons. In these series of calculations we did not transport electrons as this slows down the calculation dramatically without causing any improvement in the calculated values.

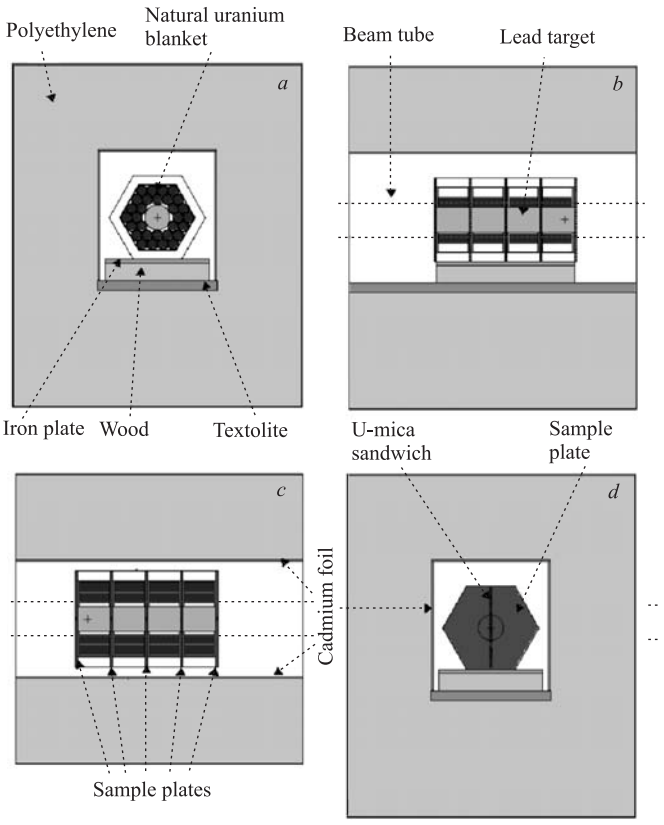

Fig. 4. The «Energy plus Transmutation» setup as seen by the MCNPX 2.6C code: *a*) XY cross section; *b*) YZ cross section; *c*) XZ cross section, and *d*) XY cross section through a sample plate and MC-fission-foils (MC-FF). The 31 MC-FFs were placed along the Y-axis. In *d*) the large circle at the centre represents the XY cross section of the hypothetical cylindrical tube of radius 6 cm, in which the proton beam is enclosed

2. Bertini intranuclear cascade (INC) model [12, 13] along with RAL fission-evaporation model [14] were used. The other available models will be considered in other parts of this paper.

3. In the case of photons, analog photonuclear particle production was used.

4. For neutrons and protons the «mix and match» option of the code was used. This option allows using the available data tables up to their upper energy limits. Then, at higher energies model calculated cross section values are used.

5. We used forced collisions in the MC-FFs to improve the statistics of the calculations.

6. High energy data tables for neutrons and protons were used whenever available [5]. Otherwise data tables of the ENDF/B-VI libraries were used.

7. In all calculations the statistical errors were less than 3% except for the case of the proton- and pion-induced fission events at large radial distances where fluxes of these particles were very low and the calculations statistics were about 6%.

2.2. Neutron Spectra. Figure 5 illustrates typical calculated neutron spectra at two radial distances ($R = 0$ cm and $R = 13.5$ cm) on plate 2 ($Z = 11.8$ cm). Figure 5, *a* shows the neutron spectra for the case when in the experimental setup both the polyethylene and Cd shields around the target-uranium assembly are present (as with the experimental setup), and Fig. 5, *b* shows a hypothetical case when both polyethylene and Cd shields are removed.

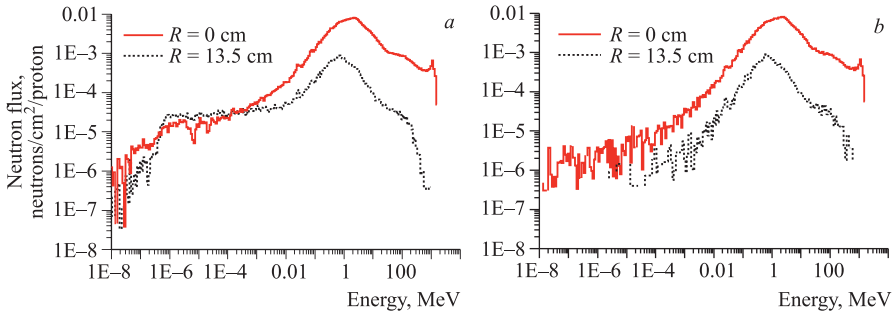

Fig. 5. Neutron energy spectra on plate 2 ($Z = 11.8$ cm) as calculated using the MCNPX 2.6C code: *a*) total system, containing the polyethylene and Cd shielding around the target-blanket assembly; *b*) hypothetical case when all material around the target-blanket assembly is removed. Equal logarithmic energy binning with 20 intervals per decade is used

From Fig. 5 it can be seen that the presence of Cd stops thermal neutrons from entering the blanket area and the combined presence of the polyethylene and Cd shields enhances the number of the neutrons relevant to resonance absorption. This simple arrangement allows us to study (a) the interaction of the neutrons with different materials in fast and resonance spectrum within the blanket area, and (b) in thermal, resonance and fast neutron spectrum within the polyethylene section of the setup. From Fig. 5, *a* it becomes clear that neutron spectrum becomes softer with increasing R.

3. RESULTS AND DISCUSSIONS

3.1. Neutron-Induced Fission. The track density ρ in units of tracks $\cdot$ cm^{-2} is related to fission-rate R_f via the following equation:

$$\rho = w \cdot R_f, \tag{1}$$

where w is a calibration factor in units of tracks $\cdot$ cm^{-2} $\cdot$ neutron^{-1} [15]. R_f is fission per atom of the fissionable nuclei in the foil induced by different particles, during the irradiation time t and is given by

$$R_f = \sum_{i=1}^{4} (R_f)_i. \tag{2}$$

$(R_f)_i$ refers to the fission-rate (fission/primary proton, during the irradiation time t) induced by particle i (which in our case are neutron, proton, pion and photon). $(R_f)_i$ is given by

$$(R_f)_i = t \cdot \int_0^\infty \varphi_i(E) \cdot \sigma_i(E) \cdot dE, \tag{3}$$

where $\varphi_i(E)$ and $\sigma_i(E)$ are the energy-dependent particle flux and fission cross section, respectively. In Eq. (2), $F_i(E) = t \cdot \varphi_i(E)$ is the energy-dependent particle fluence integrated over the irradiation time t. In this paper $F_i(E)$ will be represented as follows:

$$F_i(E) = N_p \cdot \phi_i(E), \tag{4}$$

where $\phi_i(E)$ is the energy-dependent particle flux per incident primary proton on the target and N_p is the total number of primary protons in the course of the target irradiation.

Neutrons that induce fission in the fission-foils have wide range of energies (Fig. 5) and angles of incidence with respect to the normal to the surface of the fission-foils. Figure 6 illustrates the angular distribution of the neutrons entering some of the fission-foils on plate 2 ($Z = 11.8$ cm). In Fig. 6 angular intervals $0-90$ and $90-180$ represent the neutrons that travel in forward and backward directions, respectively. For each sample the fraction of neutrons that enter the foils in forward and backward directions is shown in the figure insets.

Obviously the angular distribution and to some extent the energy spectrum of the neutrons would be different for the foils in different plates.

It is shown that [15] the calibration factor w obtained using a specific standard neutron field can be applied to an arbitrary neutron field if in the determination of w and its subsequent use the mean track density in the track detectors on both sides of a fission-foil is used.

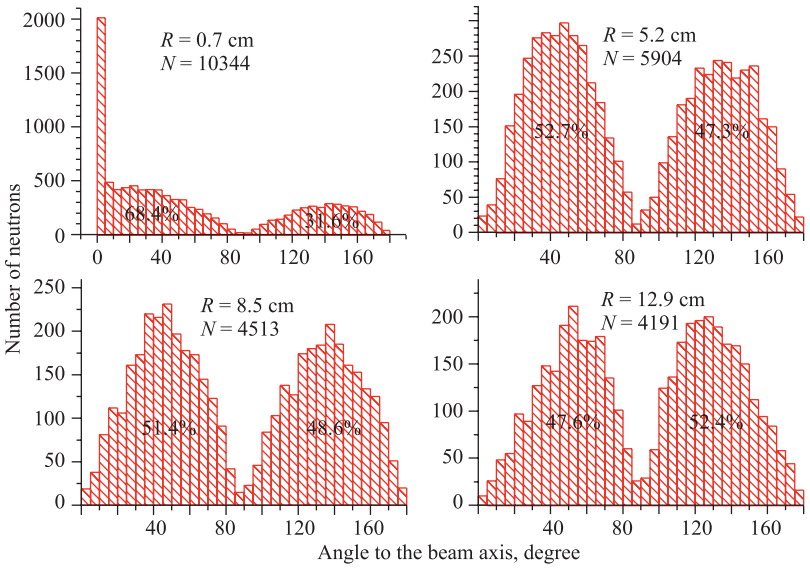

Fig. 6. Angular distribution of the neutrons that cross the front and back surfaces of MC-FFs (Fig. 2) and enter the foils at different radial distances on plate 2 as given in the figure insets. The neutron direction angles were measured with respect to the Z-axis, i.e., the target axis

Table 1 gives the mean of the track densities in the two mica detectors for each of the fission-foils, along the $+Y$-axis.

Table 1. Experimental values of mean fission track densities in the front and back mica detectors for each of the fission-foils, along the $+Y$-axis. The statistical uncertainties of the measurements are given as a percentage of the track densities

Radial distance R, cm	Track density $\times 10^5$ (tracks/cm^2)				
	Plate 1 $Z = 0$ cm	Plate 2 $Z = 11.8$ cm	Plate 3 $Z = 24.2$ cm	Plate 4 $Z = 36.4$ cm	Plate 5 $Z = 48$ cm
0	210 (±30%)	209 (±30%)	82.0 (±30%)	45.2 (±30%)	14.3 (±4%)
3	39.8 (±30%)	69.8 (±30%)	46.9 (±30%)	32.8 (±30%)	11.0 (±4%)
6	16.3 (±4%)	38.4 (±10%)	27.3 (±5%)	15.6 (±4%)	5.80 (±4%)
8.5	9.73 (±4%)	24.9 (±4%)	15.8 (±4%)	9.96 (±4%)	3.60 (±4%)
11	6.64 (±4%)	14.7 (±4%)	11.2 (±4%)	7.04 (±4%)	2.60 (±4%)
13.5	4.79 (±4%)	10.6 (±4%)	8.61 (±4%)	5.65 (±4%)	2.03 (±4%)

Using $w = (9.90 \pm 0.3) \cdot 10^{18}$ track $\cdot$ cm^{-2} $\cdot$ neutron^{-1} for thick natural uranium fission-foil and for artificial mica detector [15] and Eq. (1), the mean track densities were converted to fission-rates. It should be noted that w relates the track density in the external detector (mica) to the number of fission events within the fission-foil, regardless of the type of fission inducing particle. Also it should be noted that in the experimental determination and MC calculation of w it was assumed that all fission events are binary and the number of multiprong fission events is negligible [15]. Table 2 gives the fission-rates for $^{\mathrm{Nat}}$U samples in all radial distances and sample plates used in this study.

Table 2. Experimental values of fission-rates obtained for samples at different radial distances at different Z values. The statistical uncertainties of the measurements are given as a percentage of the fission-rates

Radial distance R, cm	Fission-rate $^{\mathrm{Nat}}\mathrm{U} \times 10^{-14}$ (fission/atom)				
	Plate 1 $Z = 0$ cm	Plate 2 $Z = 11.8$ cm	Plate 3 $Z = 24.2$ cm	Plate 4 $Z = 36.4$ cm	Plate 5 $Z = 48$ cm
0	213 (±30%)	211 (±30%)	82.9 (±30%)	45.6 (±30%)	14.5 (±4%)
3	40.2 (±30%)	70.5 (±30%)	47.3 (±30%)	33.2 (±30%)	11.1 (±4%)
6	16.5 (±4%)	38.8 (±10%)	27.6 (±6%)	15.7 (±4%)	5.86 (±4%)
8.5	9.83 (±4%)	25.1 (±4%)	15.9 (±4%)	10.1 (±4%)	3.64 (±4%)
11	6.71 (±4%)	14.8 (±4%)	11.3 (±4%)	7.12 (±4%)	2.63 (±4%)
13.5	4.84 (±4%)	10.7 (±4%)	8.69 (±4%)	5.71 (±4%)	2.05 (±4%)

In calculating the *neutron*-induced fission-rates in the MC-FFs we used the following cross-section data:

1. At neutron energies $E_n \leqslant 20$ MeV the MCNP dosimetry data libraries (see [16]) were used.

2. At $20 < E_n \leqslant 257$ MeV the fission cross-section values given by Lisowski et al. [17, 18] were used.

3. At energies $E_n > 257$ MeV the fission cross sections were calculated using the XSEX3 code from the LCS-code system [19] which comes with the MCNPX 2.6C code package. The calculated cross sections were normalized to the cross-section value of Lisowski et al. [17, 18] at 257 MeV.

Figure 7 shows the $^{238}\mathrm{U}(n, f)$ cross section as a function of neutron energy as obtained using the above procedure.

Figure 8 illustrates the experimental and calculated *neutron*-induced fission-rates as a function of the radial distance R, from the target axis (Z-axis in Fig. 2). As it can be seen the agreement between the experiment and calculation is not satisfactory, particularly at radial distances corresponding to the target region, i.e., $R \leqslant 4.2$ cm.

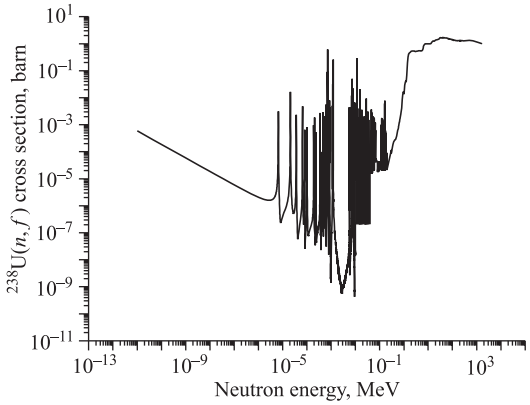

Fig. 7. $^{238}\mathrm{U}(n, f)$ cross section as a function of neutron energy (see the text for details)

3.2. Proton-, Pion-, Photon- and Muon-Induced Fission.

3.2.1. Proton-, Pion- and Muon-Induced Fission. Fission in the uranium samples and in the blanket as a whole is not only induced by secondary neutrons, but also by primary particles (protons) as well as other secondary hadrons and photons. The fission induced by particles other than neutrons can be partially responsible for the observed differences between the experimental and calculated results. Among the secondary hadrons only protons and pions are produced in significant numbers.

In these calculations possible fission events that could be induced by muons [20] have been ignored. This is for the following two reasons. Firstly, a very small number of produced muons is produced by the primary proton interactions (0.21 muons/proton). Secondly, cross-section data tables for muon-induced fission are not available.

In order to estimate the contribution of proton- and pion-induced fissions to the observed track densities, proton and pion fluxes in the MC-FFs were calculated. The particles were binned in equal logarithmic energy bins with 20 intervals per decade. Figure 9 shows the proton and pion energy distributions on plate 2 at two radial distances $R = 0$ cm and $R = 8.5$ cm.

The fission cross section for $^{\mathrm{Nat}}\mathrm{U}(p, f)$ was calculated using the best fit curve to the available experimental data as described by Prokofiev [21]. The $^{238}\mathrm{U}(\pi, f)$ cross section at different pion energies was calculated using the XSEX3 code and normalized to the experimentally determined $^{238}\mathrm{U}(\pi, f)$ cross section at pion energy of 80 MeV [22]. Figure $10, a, b$ shows the variation of the proton- and pion-induced fission cross sections of ^{238}U with the particle energy. In this paper we will assume that the (π, f) cross section for ^{238}U and $^{\mathrm{Nat}}$U is the same.

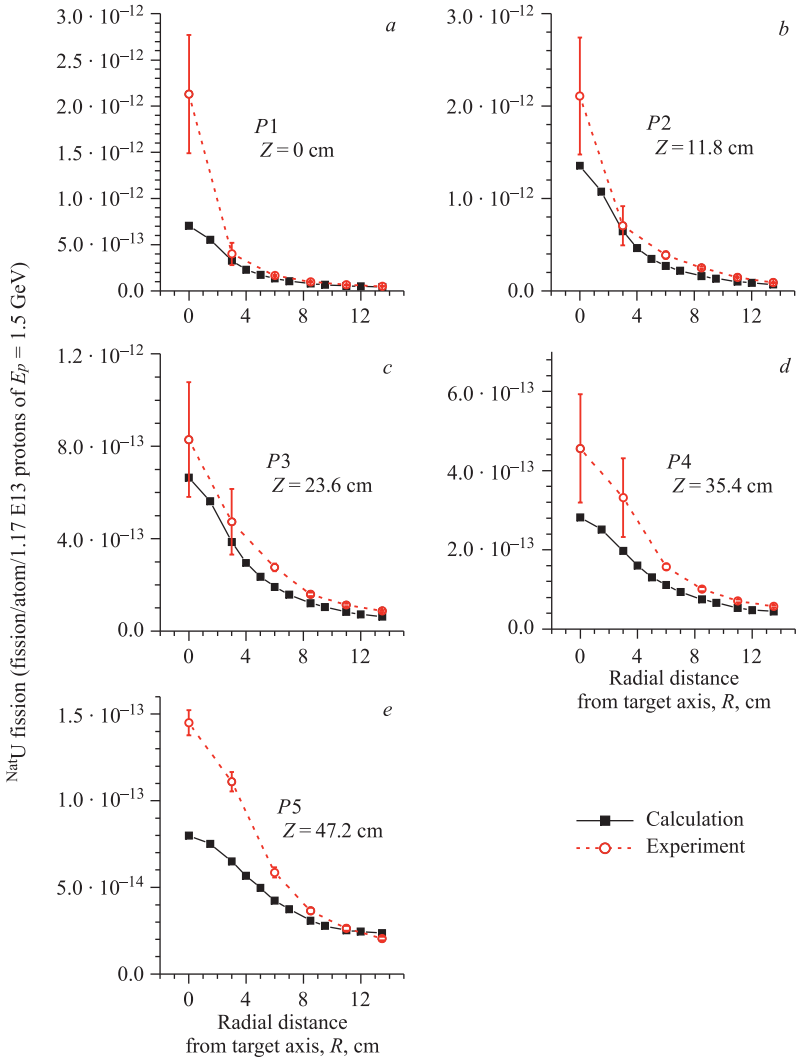

Fig. 8. Variations of $^{\mathrm{Nat}}$U fission-rate as a function of radial distance measured from the target axis. The results for five plates at different axial distances Z are shown. The calculations are only for neutron-induced fission. Note that the vertical scale ranges are not the same for all plots. Lines connecting the data points are drawn to guide the eye

Figure 10, *c, d* shows the calculated $^{\mathrm{Nat}}\mathrm{U}(p, f)$ and $^{\mathrm{Nat}}\mathrm{U}(\pi, f)$ fission-rates (fission/atom/primary proton) as a function of the radial distance for all 31 MC-FFs in each plate and for the five plates at different Z coordinates.

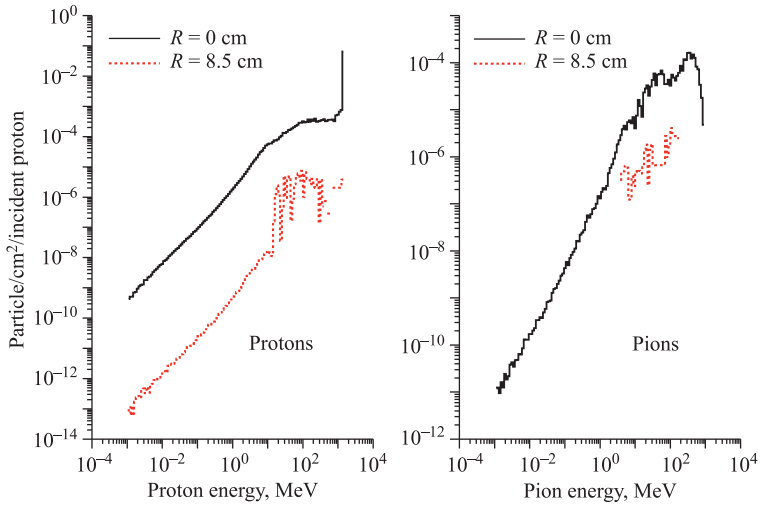

Fig. 9. Proton and pion energy spectrums on plate 2 at two radial distances $R = 0$ cm and $R = 8.5$ cm as calculated using the MCNPX code

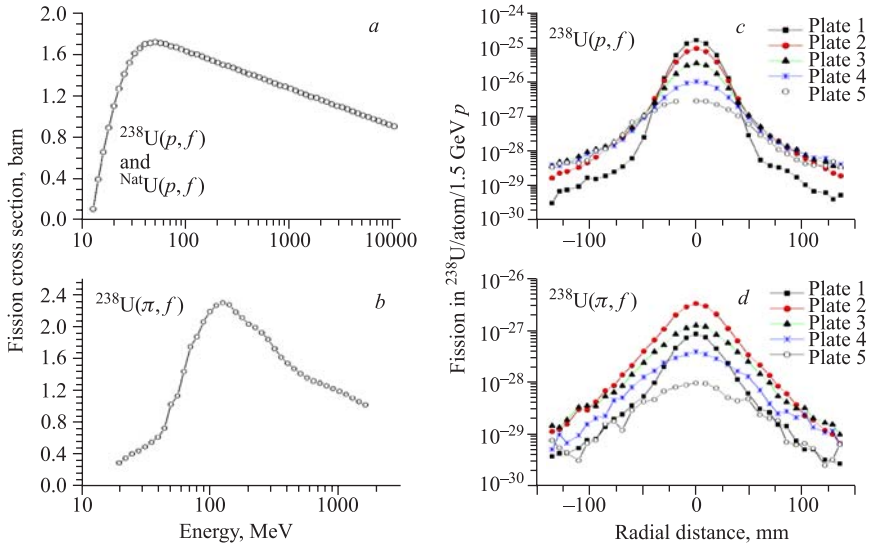

Fig. 10. (*a*) and (*b*) — cross sections for $^{\mathrm{Nat}}\mathrm{U}(p, f)$ and $^{\mathrm{Nat}}\mathrm{U}(\pi, f)$ reactions (see the text for details); (*c*) and (*d*) — $^{\mathrm{Nat}}\mathrm{U}(p, f)$ and $^{\mathrm{Nat}}\mathrm{U}(\pi, f)$ reactions rates in the «Energy plus Transmutation» setup as a function of the radial distance from the target axis for five plates at different axial distance Z. The fission-rates are expressed in units of fission/atom/(1.5 GeV p). Lines connecting the data points are drawn to guide the eye

The XSEX3 code allows the cross-section calculation at energies above 20 MeV. It is shown that the capture of pions near nuclear surface results in a deposition of approximately 80 MeV of excitation energy in the nucleus [20]. Absorption of slow pions by ^{238}U nuclei and the subsequent fission process are predominantly a symmetric division of the nucleus (see [20] and references therein). Therefore, it is expected that slow and stopping pions would induce fission in the fission-foils and in the blanket as a whole. Consequently, limiting the pion-induced fissions to energies above 20 MeV (as done in this work) will underestimate the number of such events.

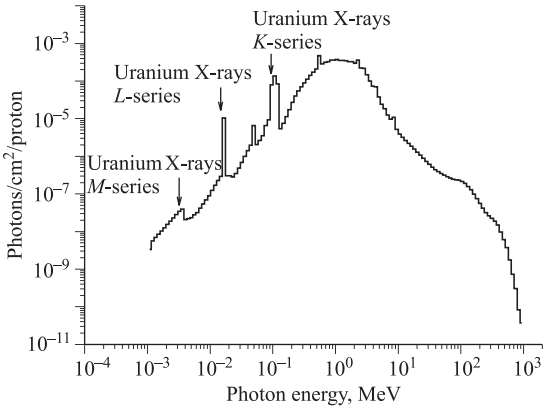

Fig. 11. Average photon flux in the blanket of the «Energy plus Transmutation» setup

3.2.2. Photon-Induced Fission. Figure 11 shows the energy distribution of the photons in the blanket as calculated using the MCNPX 2.6C code. As can be seen, the uranium X-ray peaks appear at their correct energies and spectrum extends to $\sim$ 1 GeV. It should be noted that in MCNPX calculations the correct photon spectrum will be obtained only when all elementary particles, whose production (and subsequent decay) is possible at the incident particle energy, are present in the «mode» card and are transported.

In order to estimate the photofission rates, the photon spectra in the MC-FFs were obtained and photofission rates were calculated using the photofission cross sections given in references [23–27]. Figure 12 shows the photofission cross section of ^{238}U as a function of photon energy. In using the cross-section values (Fig. 12) linear interpolation in log–log scale between the data points was used. In Fig. 12 the data points marked with arrows were not used because of their departure from the general trend of the other data point.

The sum of the calculated fission-rates induced by neutrons, protons, pions and photons in $^{\mathrm{Nat}}$U as well as the experimental results as a function of radial distance for plates at different Z coordinates are shown in Fig. 13.

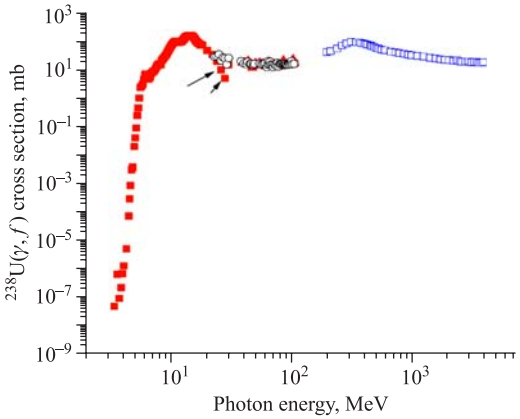

Fig. 12. ^{238}U-photofission cross section as a function of photon energy. The data were obtained from [23–27]

As it can be seen, by adding the $^{\mathrm{Nat}}\mathrm{U}(p, f)$, $^{\mathrm{Nat}}\mathrm{U}(\pi, f)$ and $^{\mathrm{Nat}}\mathrm{U}(\gamma, f)$ rates to that of $^{\mathrm{Nat}}\mathrm{U}(n, f)$, the calculated values for the fission-rate at $R < 4.2$ cm exceed the experimental results in plates at $Z = 0$ cm, $Z = 11.8$ cm and $Z = 23.6$ cm and difference between the experimental and calculation results becomes less than those shown in Fig. 8 for all data points with $R > 4.2$ cm in all sample plates.

The experimental results for R-values beyond the target radius ($R > 4.2$ cm) for which the accuracy of the track density measurements was 4% were used to determine the deviation of the experiment from the calculation. It was found that the calculated values are on average less than the experimental results by a factor of (1.22 ± 0.14).

Further analysis of the results for the blanket region suggested that the observed discrepancy between the experimental and calculated fission-rates is systematic rather than statistical. This is more evident in the log–log plot of the fission rates as a function of radial distance as shown in Fig. 14. Apart from the data points with $R > 8$ cm on plate 5, the ratio of the experimental results to their corresponding calculated values is almost constant for a given sample plate.

4. FISSION-RATE DISTRIBUTION ALONG THE TARGET AXIS

Figure 15 illustrates the variation of the $^{\mathrm{Nat}}\mathrm{U}$ fission-rate with distance along target axis for different radial distances. The trends and shapes of the distributions for experimental and calculated results are similar but the magnitudes of the fission-rates are different, as discussed earlier.

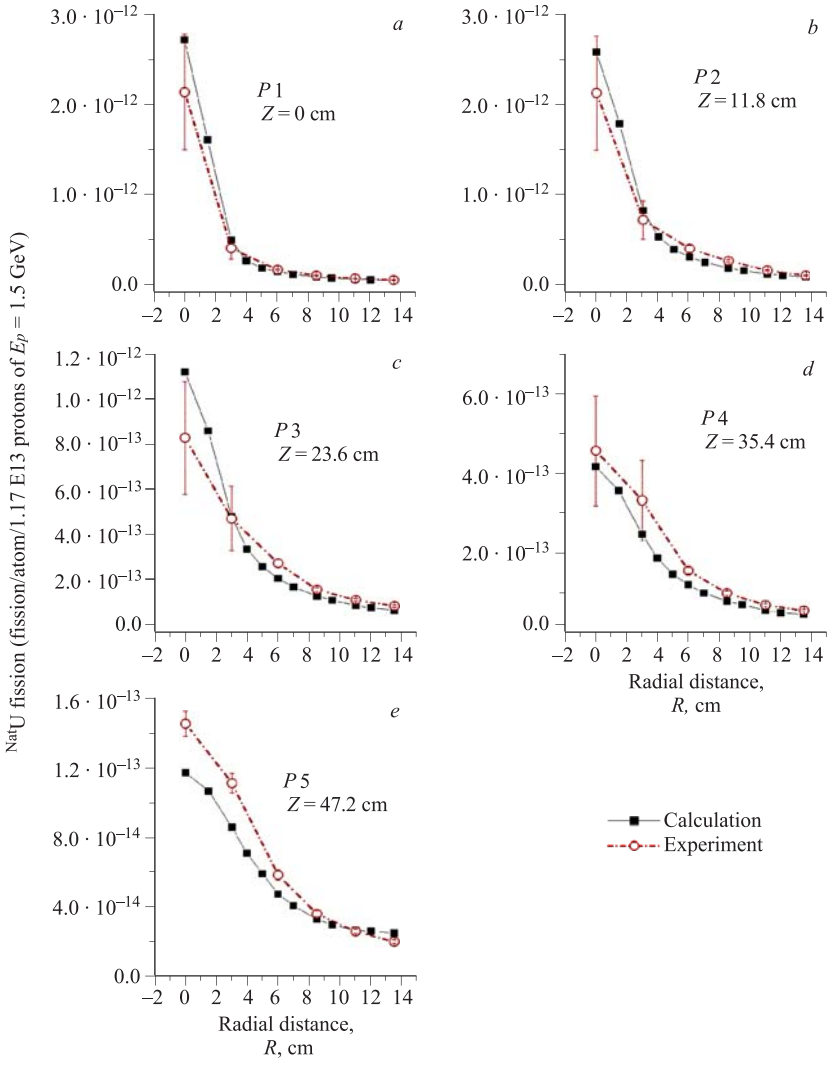

Fig. 13. Variations of the total ^{Nat}U fission-rate (includes the fission induced by neutrons, protons, pions and photons) as a function of radial distance measured from the target axis. The results for five plates at different axial distances Z are shown. Note that the vertical scale ranges are not the same for all plots and as a result the deviation between the experimental and calculated fission-rates is visually suppressed or enhanced. Lines connecting the data points are drawn to guide the eye

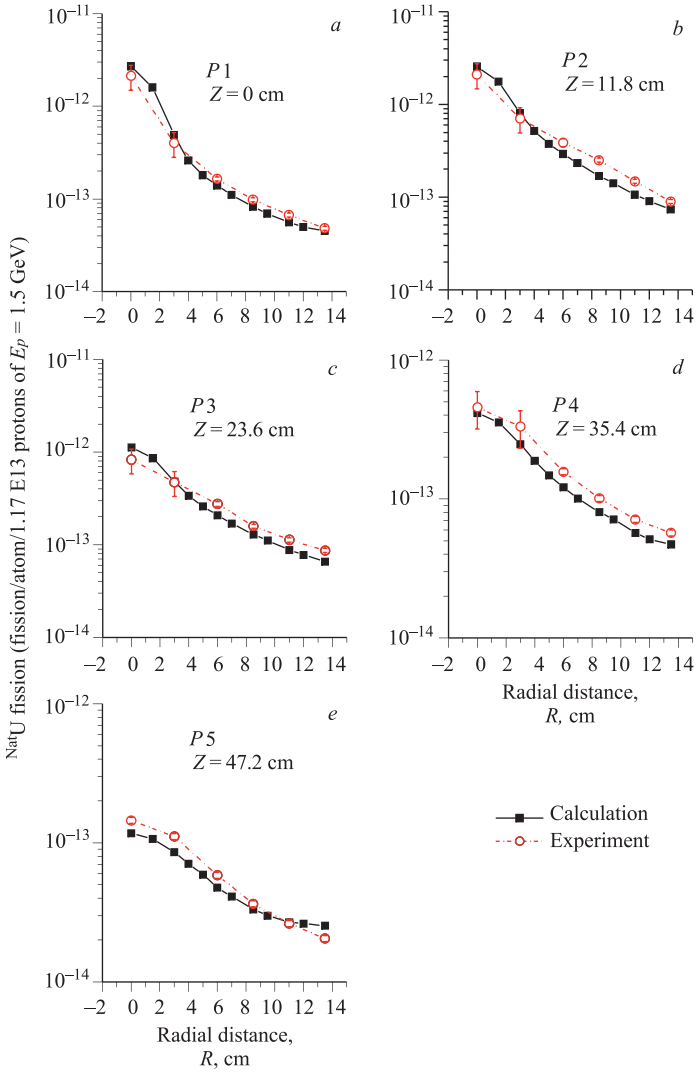

Fig. 14. Same as Fig. 13 but in log–log scales

The MC results of the fission-rate as a function of Z for each radial distance R can be fitted very well with a third order polynomial, from which the position of the maximum for each distribution can be calculated. The position maximum

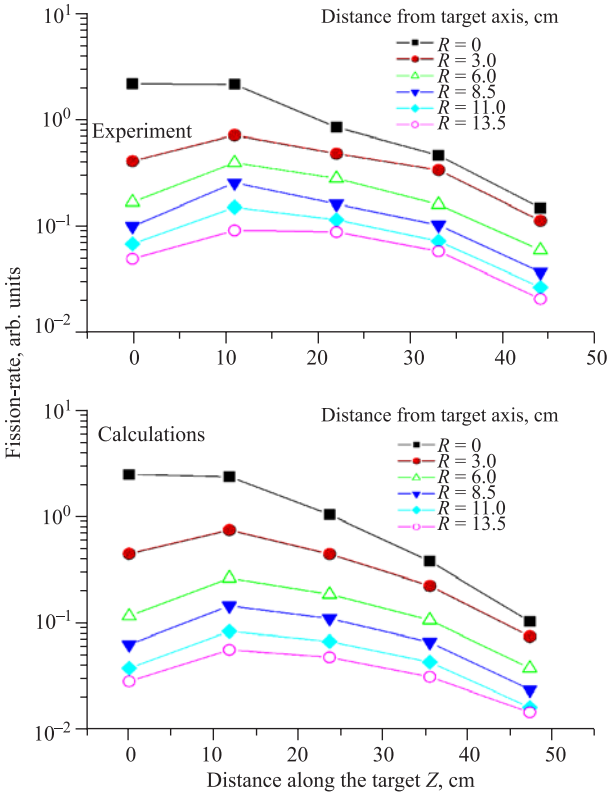

Fig. 15. Total fission-rate at different radial distances as a function of distance along the Z-axis for different radial distances R. Lines connecting the data points are drawn to guide the eye

shifts to higher Z values with increasing distance R.

5. THE OVERALL $^{\mathrm{Nat}}$U FISSION-RATE IN THE «ENERGY PLUS TRANSMUTATION» ASSEMBLY

The MCNPX 2.6C calculations show that in the whole system an interaction of one proton of energy 1.5 GeV with the target produces on average $N_{\mathrm{MC}} = 49.97$ neutrons (escaped neutrons plus captured neutrons), 8.04 protons (including the primary proton), 0.54 pions and 822.3 photons and this results in (5.73 ± 0.15) fissions in the natural uranium blanket. Further calculations showed

that contribution of the (γ, xn) reactions to the neutron population in the system is not significant. Table 3 gives the contribution of each of the particles to total number of induced fission events in the *entire blanket*.

Table 3. Contribution of different fission processes to total number of fission events in the natural uranium blanket

Fission type	Fraction of total, %
$^{\mathrm{Nat}}\mathrm{U}(n, f)$	96.76
$^{\mathrm{Nat}}\mathrm{U}(p, f)$	1.52
$^{\mathrm{Nat}}\mathrm{U}(\gamma, f)$	1.32
$^{\mathrm{Nat}}\mathrm{U}(\pi, f)$	0.40

An estimate of the total fission-rate can be made via fission-rate values calculated for the MC-FFs. We used the mean value of the fission-rates in all fission-foils along the $+Y$- and $-Y$-axes which were beyond the target but within the blanket area. We obtained mean number of (5.15 ± 0.6) fission per primary proton in the blanket. This value is in agreement with directly calculated value of (5.73 ± 0.15) as discussed above. Such an agreement indicates that if adequate number of fission-foils is distributed within a multiplying medium, the mean fission-rate in the system could be obtained from these foils.

We also calculated the number of fission events in the blanket using mean value of the fission-rates in the experimental samples in the blanket area. This resulted in total number of (6.29 $\pm$ 1.14) fission per incident proton. The large error of 18% in the experimental value of the fission-rate in the blanket is the consequence of relatively small number of the samples that were present in the blanket area (15 samples).

6. POSSIBLE SOURCES OF ERRORS

Most straightforward explanation of the observed discrepancy of 22% is possible if the difference between the experimental and calculated results could be associated with systematic errors in the calibration factor w and/or the total number of primary protons. However, on the basis of the experimental results as given in this paper and those in reference [15] we do not believe this is the case. We thus examine all possible sources of the errors in the experiments and MCNPX 2.6C calculations separately.

6.1. Experimental Errors. In obtaining the experimental results the following sources of error exist.

6.1.1. The Calibration Factor w. As the track densities in the calibration experiments [15] were in the range of $(5 \cdot 10^4 - 1.0 \cdot 10^6)$ tracks $\cdot$ cm^{-2}, track

density measurements with an error of less than 2% were possible. The other parameters used in determination of w were the neutron fluence from standard neutron sources with well-known fluxes having errors of less than 2% and well-known experimentally determined fission cross sections for ^{235}U and ^{238}U at energies of thermal and 14.7 MeV. The overall error in w was estimated to be 3%.

6.1.2. Track Density Measurements. The error in the track density measurements is dependent on the track population in a given sample. For track densities in the range of $(10^4-3\cdot10^6)$ the error was 2% at 1σ. In these samples more than 2500 tracks per mica detector were counted. In the samples with track density in the ranges of $(4-7)\cdot10^6$ and $(0.8-2)\cdot10^7$ the estimated counting error was 30% and $(30-50)$%, respectively. Such high error values for these types of samples result from the fact that in highly populated samples large numbers of tracks overlap and result in underestimation of the track densities. This is responsible for the observed underestimation of the experimental fission-rates in the fission-foils at $R < 4.2$ cm in sample plates at $Z = 0$ cm, $Z = 11.8$ cm and $Z = 23.6$ cm as shown in Figs. 13 and 14.

6.2. Errors in Monte-Carlo Calculations.

6.2.1. Effects of the Intranuclear Cascade and Fission-Evaporation Models. In the preceding calculations the Bertini intranuclear cascade and RAL fission-evaporation models have been used. To examine the effects of all other available models we performed the following calculations:

1. Net neutron production in the system (captured + escaped neutrons) was calculated.

2. The fission-rate (number of fission events in whole blanket per incident proton) was calculated for two energy groups of $E_n \leqslant 20$ MeV and $E_n > 20$ MeV. The cross-sections data libraries were same as for earlier calculation. The number of fissions induced by particles other than neutron was calculated using the procedures described in Subsec. 3.2 of this paper.

3. Calculations were performed for INC models of Bertini [12, 13], INCL4 [28] and CEM03 [29, 30] in combination with RAL [14], ORNL [31] and ABLA [32] fission-evaporation models. It should be mentioned that CEM03 is a self-contained package and fission-evaporation model is built into the code [6, 29, 30].

Table 4 shows the results. The statistical uncertainties of the calculations were less than 2%. Although within the experimental uncertainties all of the calculated overall fission-rates are in agreement with the experimental fission-rate in the blanket (i.e., 6.29 ± 1.14), it seems that the best agreement is obtained for the case of Bertini + ABLA models and the CEM03 model. The last column of Table 4 gives the ratio of the calculated values of the fission-rate R_{MC} to the experimental fission-rate R_{exp} in the blanket. It was found that if Bertini + ABLA models were used instead of Bertini + RAL models, then the deviation between

Table 4. Net neutron yield and number of fission events in the natural uranium blanket of the «Energy plus Transmutation» setup per incident proton of $E_p = 1.5$ GeV. Calculations were performed using the MCNPX code with different INC physics and fission-evaporation models

INC physics model	Fission-evaporation model	Net neutron yield (neutrons/ proton)	Neutron-induced fission per proton		Overall fission per proton, R_{MC}	$R_{\mathrm{MC}}/R_{\mathrm{exp}}$
			$E_n \leqslant 20$ MeV	Total		
BERTINI	RAL	49.97	4.55	5.54	5.73	0.91 ± 0.17
	ORNL	52.66	4.82	5.85	6.04	0.96 ± 0.17
	ABLA	52.92	5.02	6.03	6.23	0.98 ± 0.18
INCL4	RAL	43.75	3.77	4.88	5.04	0.80 ± 0.15
	ORNL	45.61	3.98	5.12	5.29	0.84 ± 0.15
	ABLA	47.07	4.32	5.46	5.65	0.90 ± 0.16
CEM03	–	52.91	4.96	5.94	6.14	0.98 ± 0.18

the experimental and calculated fission-rates in the *foils* in the blanket region will be reduced from 22 to 13%.

6.2.2. Effects of the Beam Centre Position. The error in beam centre coordinates (X_c, Y_c) on the target cannot exceed half of the width of the lead-mica sandwich sample placed at the center of plate 1 (i.e., 0.35 cm). In order to investigate the effects due to variation in the beam centre coordinates on the calculated fission-rates and their spatial distribution, several calculations with different (X_c, Y_c) sets were performed. Figure 16, *a* illustrates the fission-rate distribution along the Y-axis on plate 5. The vertical axis in Fig. 16, *a* refers to the sum of neutron-, proton-, pion- and photon-induced fissions in the MC-FFs. This figure shows the fission-rates for cases in which the beam centre is moved in positive Y-direction (along which the experimental samples were positioned).

Calculations showed that on the average fission-rates in samples along the $+Y$-axis and in the blanket area increase by 5.5% for ($X_c = 0$ cm, $Y_c = 0.5$ cm), by 4% for ($X_c = 0.5$ cm, $Y_c = 0.5$ cm) and by 11.8% for ($X_c = 0$ cm, $Y_c = 1$ cm) as compared with the case of ($X_c = 0$ cm, $Y_c = 0$ cm).

Therefore, considering the maximum error in the values of the beam centre coordinates (0.35 cm) we conclude that errors on X_c and Y_c cannot introduce more than 5% error in the calculated fission-rates.

6.2.3. The Beam Angle with Respect to the Target Axis. If the target axis was not perfectly parallel with the proton beam axis, then this will cause the beam

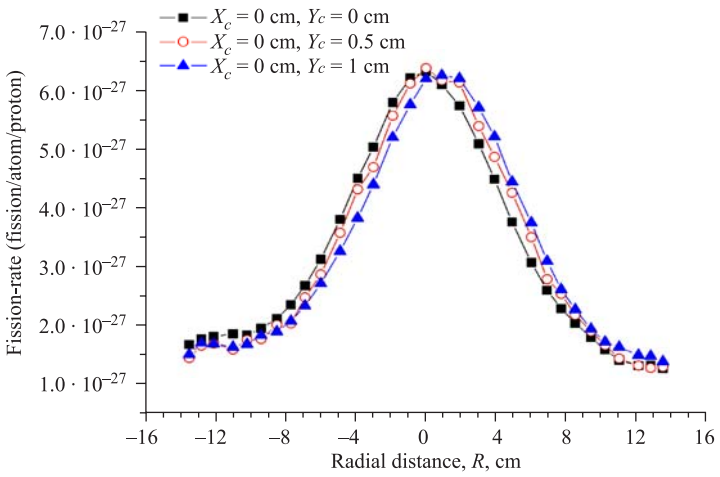

Fig. 16. Total induced fission in U-foils of plate 5 ($Z = 47.2$ cm) for three different beam centre coordinates of (0, 0), (0, 0.5) and (0, 1). Lines connecting the data points are drawn to guide the eye

centre to move away from the target axis with different amounts at different Z positions along the target, regardless of how perfectly the beam centre coincides with target centre at $Z = 0$ cm. Assuming an angle of $0.5-1$ deg between the beam and target axes on plane YZ (Figs. $1, a$, $2, c$ and $4, b$), which must have been easily detectable in the course of the experiment setup and beam alignment, the maximum beam centre shift will be $0.41-0.84$ cm at the position of plate 5 ($Z = 47.2$ cm). Calculations showed that such an error on the beam direction cannot cause an average error of more than 5% on the calculated fission-rates.

6.2.4. Effects of Neutron Energy Spectrum. Obviously the neutron energy spectrum and its hardness at the position of the MC-FFs and in the blanket as a whole can affect the fission-rates. The neutron spectrum within the blanket is determined by 1) the spallation neutron spectrum, 2) the uranium fission neutron spectrum, 3) the spectrum of neutrons from (*n, xn*) reactions, and 4) the material present in the setup and to some extent by the material present in the laboratory environment. In the calculations one can introduce error only via variations in the material compositions and their geometrical arrangements in the code. The Pb target and uranium blanket were properly built into the code as is evident from Fig. 4. Only some minor approximations were introduced on the geometrical arrangements of the granulated polyethylene shield around the target and on the laboratory environment and its content (cf. Fig. $1, a, b$ with Fig. $4, a, b$, respectively). Effects of these approximations on the calculated fission-rates will be investigated in the following paragraphs.

To examine the effects of the granulated polyethylene (around the target-blanket assembly) on the $^{\mathrm{Nat}}$U fission-rate in the blanket the average density of granulated polyethylene (0.7 $\mathrm{g \cdot cm^{-3}}$) was altered and the fission-rate in the blanket was calculated.

Calculations showed that a variation of the polyethylene density from 0.5 to 0.9 $\mathrm{g \cdot cm^{-3}}$ (i.e., changing of its mass from 215 to 388 kg) does not change the neutron-induced fission-rate in the natural uranium blanket by more than the statistical uncertainties of the calculations which were less than 3%. In the extreme case when all material around the target-blanket was totally removed (see Fig. 5, *b*), the neutron-induced fission-rate in the blanket was reduced only by 7.3% presumably due to fission in the ^{235}U component of natural uranium.

In our calculations we added a heavy concrete spherical shell of diameter 8 m and two different thicknesses of 0.5 and 1 m around the «Energy plus Transmutation» setup to take into account the effects of material present in the laboratory and in the walls of the irradiation hall on the neutron spectrum and the calculated fission-rates. In both cases this addition did not alter the results noticeably.

CONCLUSIONS

The fission-rate of $^{\mathrm{Nat}}$U in the «Energy plus Transmutation» subcritical experimental setup was measured using fission track technique for incident proton energy of 1.5 GeV. The MCNPX 2.6C code was used for transport and simulation of the interactions of the primary and secondary particles in the system.

It is shown that proton-, pion- and photon-induced fissions contribute significantly to the total fission-rate in the samples within the target volume and its immediate vicinity. The contribution of proton-, pion- and photon-induced fissions to the overall number of fission events in the blanket does not exceed 1.52, 0.40 and 1.32%, respectively.

On the basis of the experimental and theoretical results given in this paper it is evident that in the «Energy plus Transmutation» setup the fission-rate of $^{\mathrm{Nat}}$U in the blanket is *not* too sensitive to the modifications introduced to the neutron energy spectrum because of the materials beyond the Cd shielding (Fig. 1). This is due to the fact that, because of the small size and material composition of the target-blanket and samples present in the setup, the neutron energy spectrum is not significantly changed by these modifications. Obviously this will not be the case for isotopes such as ^{235}U for which fission cross section in the thermal, epithermal and resonance regions of the neutron spectrum is much higher than that for $^{\mathrm{Nat}}$U.

The beam centre coordinates affect the spatial distribution of the secondary particles in our experimental setup, however this effect will not be too important

when targets with larger diameters are used (especially for positions beyond the target radius); a situation expected to be the case in a realistic ADS.

It is shown that the MCNPX 2.6C code prediction of the fission-rate is consistently lower (by 22%) than the experimental value for the fission-foils placed in the blanket region, when the Bertini and RAL models are used in the calculations. This deviation reduces to $\sim 13\%$ when the Bertini and ABLA models or CEM03 model are used instead.

From the experimental fission-rate measurements the total number of fission events in the whole blanket was estimated as (6.29 ± 1.14) (fission/proton), which is 22% higher than the value calculated using the MC-FFs and Bertini + RAL models. Direct calculation of fission-rate in the blanket using different INC and fission-evaporation models given in Table 4 showed that the best agreement between the experiment and calculation is obtained when Bertini INC model in combination with ABLA fission-evaporation model are used. Also, the MC results obtained using CEM03 INC model are in good agreement with the experimental results.

Acknowledgements. We would like to thank Veksler and Baldin Laboratory of High Energy Physics (VBLHEP), Joint Institute for Nuclear Research (JINR), Dubna, Russia and staff of the Nuclotron accelerator for providing us with the research facilities used in these experiments. Some of us would like to thank JINR for the hospitality during their stay in Dubna. SRH-N would like to thank the Department of Education, Science and Training of the Government of Australia for the AMRFP grant and the School of Physics, University of Sydney for Denison research grant in support of this work.

REFERENCES

1. *Bowman C. D. et al.* // Nucl. Instr. Meth. A. 1992. V. 320. P. 336.
2. *Rubbia C. et al.* Fast Neutron Incineration in the Energy Amplifier as Alternative to Geological Storage: The Case of Spain, CERN/LHC/97-01, 1997.
3. Physics and Safety of Transmutation Systems, A Satus Report. OECD 2006, NEA No. 6090, ISBN 92-64-01082-3.
4. *Hashemi-Nezhad S. R. et al.* // Kerntechnik. 2001. V. 66. P. 47.
5. *Chadwick M. B. et al.* // Nuclear Science and Engineering. 1999. V. 131. P. 293.
6. *Hendricks J. S. et al.* MCNPX, VERSION 26C, Repot LA-UR-06-7991, Los Alamos National Lab. Dec. 7, 2006.
7. *Krivopustov M. I. et al.* JINR Preprint P1-2000-168. Dubna, 2000; *Krivopustov M. I. et al.* // Kerntechnik. 2003. V. 68. P. 48–55.

8. *Westmeier W. et al.* // Radiochimica Acta. 2005. V. 93. P. 65.

9. *Wan J.-S. et al.* // Nucl. Instr. Meth. B. 1999. V. 155. P. 419.

10. *Krivopustov M. I. et al.* JINR Preprint E1-2004-79. Dubna, 2004.

11. *Prokofiev A. V., Mashnik S. G., Sierk A. J.* Cascade-Exciton Model Analysis of Nucleon-Induced Fission Cross Section of Lead and Bismuth at Energies 45 to 500 MeV. nucl-th/9802027 v1. 9 Feb. 1998; LA-UR-98-0418, LANL, Los Alamos. 1998.

12. *Bertini H. W.* // Phys. Rev. 1963. V. 131. P. 1801.

13. *Bertini H. W.* // Phys. Rev. 1969. V. 188. P. 1711.

14. *Atchison F.* Targets for Neutron Beam Spallation Sources. Jul-Conf-34, Kernforschungsanlage Julich GmbH. Jan. 1980.

15. *Hashemi-Nezhad S. R. et al.* // Nucl. Instr. Meth. in Phys. Res. A. 2006. V. 568. P. 816.

16. MCNP-4B, A General Monte Carlo N-Particle Transport Code / Ed. Briesmeister J. F. Report LA-12625, Los Alamos National Lab. 1997.

17. *Lisowski P. W. et al.* // Proc. of the Specialists' Meeting on Neutron Cross Section Standards for the Energy Region above 20 MeV, OECD/NEA Report NEANDC-305 «U», Uppsala, Sweden, 1991. P. 177.

18. *Lisowski P. W. et al.* // Proc. of Nuclear Data for Science and Technology, Jülich, Germany, 1991. Berlin: Springer-Verag, 1992. P. 268.

19. *Prael R. E., Lichtenstein H.* User Guide to LCS: The LAHET Code System. Report No. LA-UR-89-3014. Los Alamos National Lab. 1989.

20. *Budick B. et al.* // Phys. Rev. Lett. 1970. V. 24. P. 604.

21. *Prokofiev A. V.* // Nucl. Instr. Meth. A. 2001. V. 463. P. 557.

22. *Khan H. A., Khan N. A., Peterson R. J.* // Phys. Rev. C. 1987. V. 35. P. 645.

23. *Varlamov V. V. et al.* Fotojad. Dannye-Photofission of U-235,238. Moscow State Univ., Nucl. Phys. Inst. M., 1987.

24. *Cetina C. et al.* // Phys. Rev. C. 2002. V. 65. P. 044622.

25. *Ries H. et al.* // Phys. Lett. B. 1984. V. 139. P. 254.

26. *Leprêtre A. et al.* // Nucl. Phys. A. 1987. V. 472. P. 533.

27. *Neto J. D. A. et al.* // Phys. Rev. C. 1976. V. 14. P. 1499.

28. *Boudard A. et al.* // Phys. Rev. C. 2002. V. 66. P. 044615.

29. *Mashnik S. G., Sierk A. J.* Recent Developments of the Cascade-Exciton Model of Nuclear Reactions, Los Alamos National Lab. Report LA-UR-01-5390, and International Conference on Nuclear Data for Science and Technology, Tsukuba, Japan, October 7–12, 2001.

30. *Mashnik S. G. et al.* CEM03.S1, CEM03.G1, LAQGSM03.S1, and LAQGSM03.G1 Versions of CEM03.01 and LAQGSM03.01 Event-Generators, Los Alamos National Lab. Report LA-UR-06-1764. 2006.

31. *Barish J. et al.* HETFIS High-Energy Nucleon-Meson Transport Code with Fission, Oak Ridge National Lab. Report ORNL-TM-7882. 1981.

32. *Junghans A. R. et al.* // Nucl. Phys. A. 1998. V. 635. P. 428.

Received on April 23, 2008.

Редактор *В. В. Булатова*

Подписано в печать 06.03.2009.
Формат 60 × 90/16. Бумага офсетная. Печать офсетная.
Усл. печ. л. 1,81. Уч.-изд. л. 2,46. Тираж 370 экз. Заказ № 56531.

Издательский отдел Объединенного института ядерных исследований
141980, г. Дубна, Московская обл., ул. Жолио-Кюри, 6.
E-mail: publish@jinr.ru
www.jinr.ru/publish/